

www.acsami.org Research Article

Plasma-Induced Catalytic Conversion of Nitrogen and Hydrogen to Ammonia over Zeolitic Imidazolate Frameworks ZIF-8 and ZIF-67

Fnu Gorky, Jolie M. Lucero, James M. Crawford, Beth Blake, Moises A. Carreon, and Maria L. Carreon*



Cite This: ACS Appl. Mater. Interfaces 2021, 13, 21338–21348



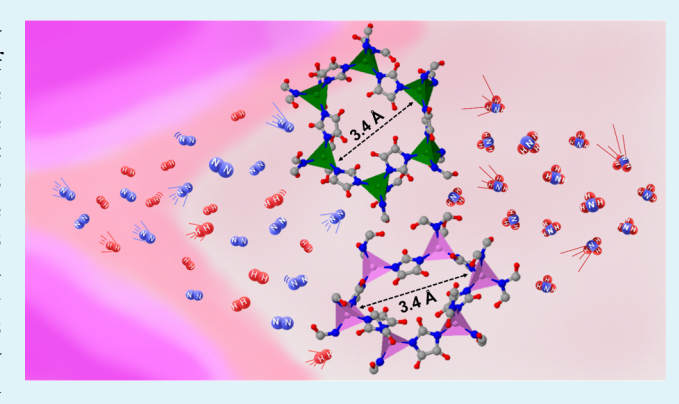
ACCESS

Metrics & More



s Supporting Information

ABSTRACT: Microporous crystals have emerged as highly appealing catalytic materials for the plasma catalytic synthesis of ammonia. Herein, we demonstrate that zeolitic imidazolate frameworks (ZIFs) can be employed as efficient catalysts for the cold plasma ammonia synthesis using an atmospheric dielectric barrier discharge reactor. We studied two prototypical ZIFs denoted as ZIF-8 and ZIF-67, with a uniform window pore aperture of 3.4 Å. The resultant ZIFs displayed ammonia synthesis rates as high as 42.16 μ mol NH₃/min gcat. ZIF-8 displayed remarkable stability upon recycling. The dipole—dipole interactions between the polar ammonia molecules and the polar walls of the studied ZIFs led to relatively low ammonia uptakes, low storage capacity, and high observed ammonia synthesis rates. Both ZIFs outperform other microporous crystals including zeolites and



conventional oxides in terms of ammonia production. Furthermore, we demonstrate that the addition of argon to the reactor chamber can be an effective strategy to improve the plasma environment. Specifically, the presence of argon helped to improve the plasma uniformity, making the reaction system more energy efficient by operating at a low specific energy input range allowing abundant formation of nitrogen vibrational species.

KEYWORDS: nonthermal plasma, plasma catalysis, ammonia synthesis, zeolitic imidazolate frameworks, ammonia adsorption effect

■ INTRODUCTION

Ammonia is an essential chemical in the food market due to its importance in the production of fertilizers. The industrial production of ammonia is currently done using the Haber-Bosch (HB) process which occurs at ~500 °C and 500 bar, making it the most energy-intense process in the chemical industry. The worldwide ammonia production averages ~249.4 million tons which results in the consumption of $\sim 1-2\%$ of the world's energy and 2-3% of the planet's natural gas output. Moreover, the HB process results in the emission of over 300 million metric tons of CO₂. 1,2 This excessive energy requirement makes the HB process economically feasible only at a large scale, requiring vast capital investments and continuous electric power supply to maintain a continuous process.^{3,4} Subsequently, centralized ammonia synthesis hinders the access to affordable fertilizers to farms in remote areas.5 The development of alternative technologies to the HB process at milder conditions and compatible with intermittent electricity from renewable sources is a critical step for small-scale, decentralized ammonia production. Explored alternatives include decoupling dissociation of H2 and N2 in membrane reactors⁶ or by proton-based activation of N₂ in electrochemical cells. Electrochemical ammonia synthesis has been motivated by the possibility of low-cost renewable electricity

(commercial solar power plummeted from \$5.36/W in 2010 to \sim \$1.85/W in 2017). The main issue with electrochemical N₂ reduction is its limited selectivity as H₂ is overwhelmingly the preferred product, with current efforts focused on addressing this issue. It is the cost-effective implementation of solar and wind sources observed in the past decade that has motivated the search for sustainable alternatives. The realization of this technology to fully replace fossil fuels for electricity, heat, and transportation will be only feasible when there is effective energy storage and distribution technology. Plasma catalysis is an unconventional and transformative route that takes advantage of renewable electricity, providing an alternative that can lead to the future prospect of the electrification of the chemical industry. 11

Currently, the rational engineering of a catalyst for cold plasma environments is emerging as a highly promising strategy to lead to a sustainable route to produce ammonia.¹²

Received: February 16, 2021 Accepted: April 18, 2021 Published: April 28, 2021





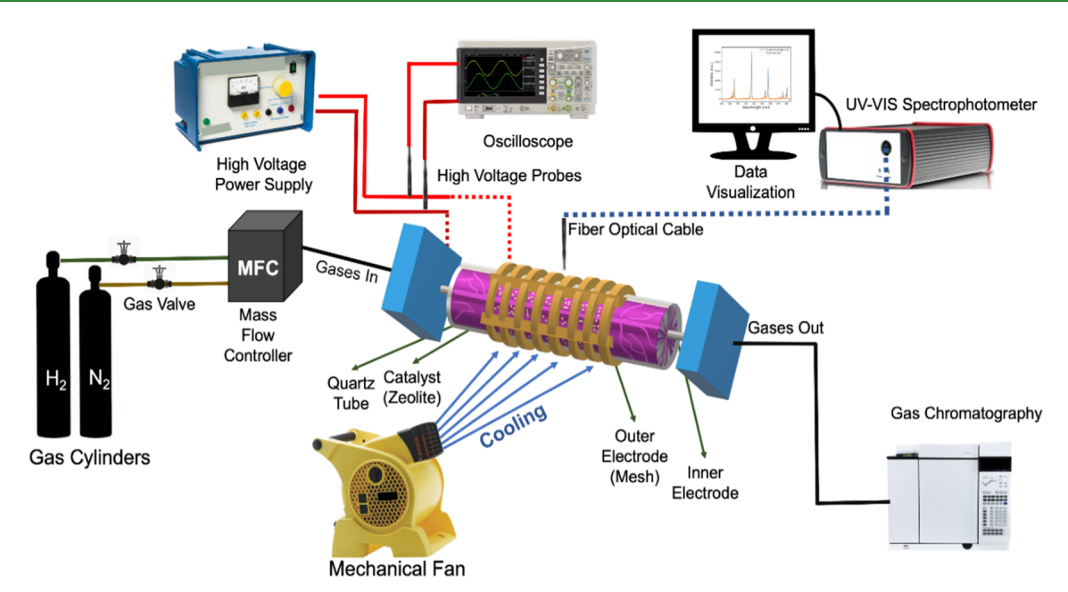


Figure 1. Schematic of the DBD reactor employed in this study.

Specifically, the high-energy electrons in plasmas can excite ground-state molecules that can react on the surface of selected materials at thermal efficient conditions and lower pressures compared to those in traditional catalysis.¹³ The presence of a suitable active catalyst for plasma environments can enhance ammonia production and selectivity.^{14–22} Despite all these possible benefits of plasma catalysis, our current knowledge of proper catalysts for such purposes is very limited. Furthermore, there is a need to have a better understanding of how different materials behave when exposed to plasma due to the emergence of plasma-awakened properties or interactions. In this contribution, we explore the synergy between ammonia production and ammonia adsorption (storage) over two zeolitic imidazolate frameworks (ZIFs).

The use of crystalline porous phases displaying unimodal micropores is highly appealing for plasma ammonia synthesis and also in other sustainable applications. ^{23,24} Recently, our group illustrated the use of microporous crystalline materials, including metal—organic frameworks²⁵ and zeolites, ^{26,27} as competitive catalysts for plasma catalytic ammonia synthesis. We found that pore size plays a prominent role in catalytic performance. Prompted by the observed significance of the pore size, in this work, we demonstrate that microporous crystalline phases with reduced crystallographic restrictive pore apertures catalytically outperform microporous crystals having larger pore sizes and traditional porous oxides. Specifically, we focus on two representative microporous molecular sieve crystals, ²⁸ ZIF-8 and ZIF-67, having a pore window of ~3.4 Å.

■ EXPERIMENTAL METHODS

Synthesis of Zeolitic Imidazolate Frameworks. Synthesis of ZIF-8. ZIF-8 crystals were prepared as reported elsewhere. First, the metal solution was prepared by dissolving 0.2 g of zinc chloride (Acros, 97%) and 0.3 g of sodium formate (Sigma-Aldrich, >99%) in 10 g of methanol (Fisher Scientific, 99.9%). The organic solution was prepared by dissolving 0.96 g of 2-methylimidazole (Sigma-Aldrich, 99%) in 10 g of methanol. The two solutions were then mixed together vigorously for 30 min at room temperature and then added to a Teflon-lined stainless steel autoclave and solvothermally treated for 4 h at 120 °C. The autoclave was then cooled naturally, and the ZIF-8 powder was recovered by centrifugation and washed 3× with clean methanol. The powder was then dried at 100 °C.

Synthesis of ZIF-67. ZIF-67 crystals were synthesized by a slightly different approach as reported elsewhere. 30 5 g of 2-methylimidazole (Sigma-Aldrich, 99%) was dissolved in 20 mL of deionized (DI) water. In a second solution, 0.23 g of cobalt(II) nitrate hexahydrate (Sigma-Aldrich, 98%) was dissolved in 3 mL of DI water. The two solutions were then mixed together vigorously for 15 h at room temperature. ZIF-67 was then recovered through centrifugation, washed $4\times$ with clean DI water, and dried in an oven at $100\,^{\circ}\mathrm{C}$.

Characterization Methods. Powder X-ray diffraction patterns were collected on a Siemens Krystalloflex 810, operated at 25 mA, and 30 kV. Scanning electron microscopy images were collected on a JEOL-7000 JSM field-emission microscope operated at accelerating voltages of 8–15 kV. ZIF samples were gold sputter-coated to prevent charging. Ammonia isotherms were collected on an ASAP 2020 apparatus (Micromeritics) equipped with corrosion-resistant Kalrez O-rings (DuPont). Prior to analysis, ZIF-8 and ZIF-67 were degassed under vacuum at 200 °C. A vacuum-insulated Dewar with an ice bath at 273 K with equilibration times of at least 10 min was used for all samples.

Nitrogen isotherms were obtained on an ASAP 2020 Plus (Micromeritics) using a liquid nitrogen bath (77 K). All samples were degassed for 8 h at 200 $^{\circ}$ C under high vacuum conditions. Once degassed, the final sample weight was recorded. All samples were again degassed under high vacuum for 2 h on the analysis port prior to data acquisition. Surface areas were calculated using the Brunauer–Emmett–Teller method.

Reactor Setup. The catalytic activity of the studied ZIFs was evaluated in a customized dielectric barrier discharge (DBD) reactor described in our previous reports. 26,27,31 The experimental setup consists of the reactor core, the OES (optical emission spectrum) setup, an oscilloscope to measure electrical properties, and a gas chromatograph to follow reaction products. The experimental arrangement is shown in Figure 1. During the catalytic tests, the reactor chamber is filled with nitrogen and hydrogen. The reactor exhaust is connected directly to an Agilent 7820A GC operating with a HP-PLOT U column (30 m \times 0.32 mm \times 10 μ m) with hydrogen gas as a carrier. To ensure that all ammonia is captured, the gas was bubbled in deionized water. This also provides an alternate method of quantification. The power supply was connected to the reactor using Litz wire and clips. The inner electrode is made of tungsten (2.4 mm diameter), and it is placed at the center of a quartz tube (I.D. of 4 mm and O.D. of 6.40 mm). Perfluoroalkoxy fittings were employed to avoid arc formation. The outer electrode, made of tinned copper mesh, acts as a ground electrode. The plasma length extends to ~8 cm. The impedance was matched to deliver maximum power. The gases passed through the annular section. A couple of quartz frits were

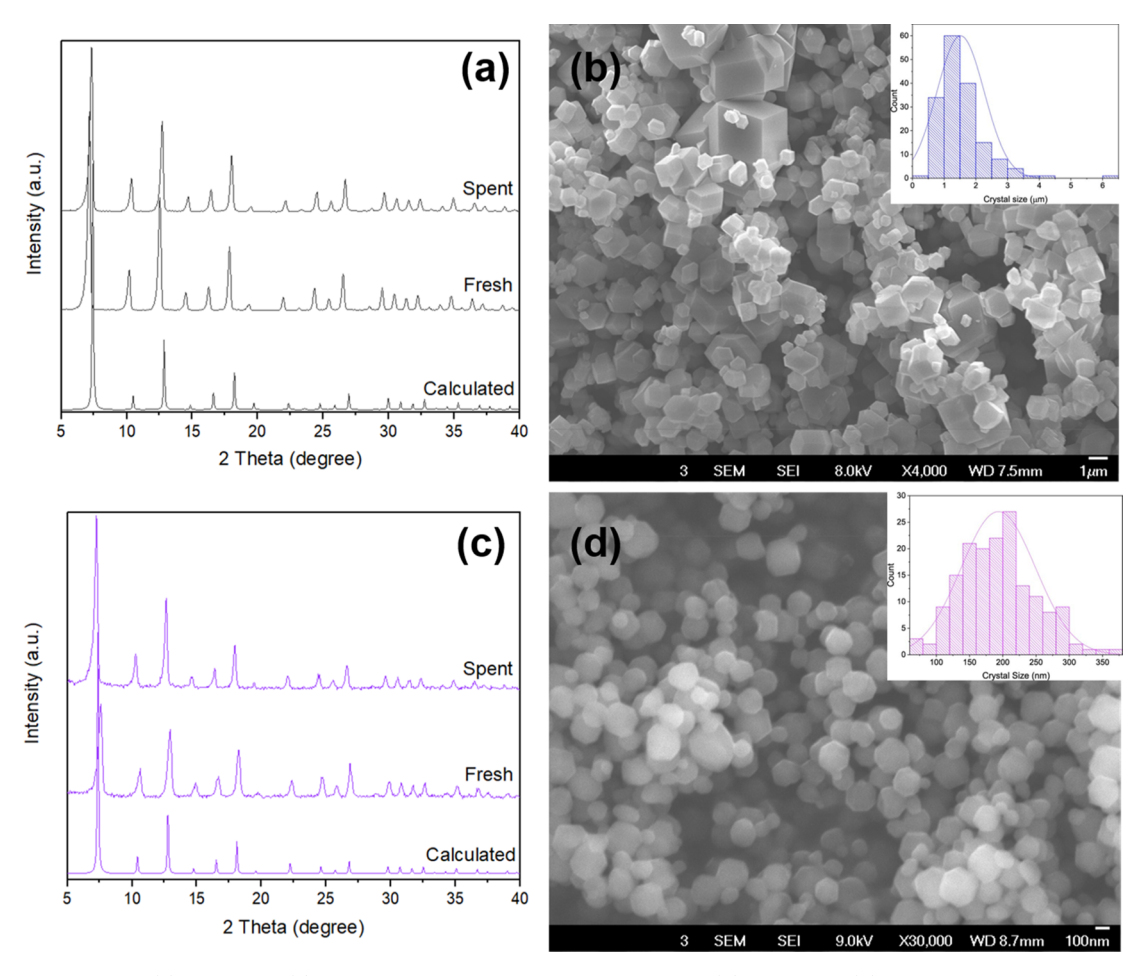


Figure 2. XRD patterns of (a) ZIF-8 and (c) ZIF-67 and representative SEM images of (b) ZIF-8 and (d) ZIF-67 microporous crystals employed as catalysts in this study. Insets correspond to histograms showing crystal size distribution.

placed carefully to avoid catalyst displacement without causing a pressure increase. A total catalyst mass of 100 mg was loaded in the reactor. A mixture of nitrogen and hydrogen was passed to homogenize the chamber after sealing the reactor. The plasmacatalyst intersection has an approximate length of 6 cm. The catalyst was packed in the overlap between the inner and outer electrodes. The reactions were carried out at different flow ratios ranging from 3:1 to 1:6 ratio of nitrogen to hydrogen (N_2/H_2) with a total flow rate of 25 sccm at different voltages ranging from 7 to 21 $kV_{pk-pk}.$ The average bulk temperature of the reactor was 98 °C (± 1.2 °C) maintained with the use of a fan continuously running during the reaction time. The ammonia yield denotes the degree of nitrogen fixation compared to the nitrogen fed. The yield was calculated by taking the ratio of the ammonia synthesis rate to the nitrogen flow rate fed on a molar basis. To determine the ammonia synthesis rate, a calibration curve was built. Details are provided in Table S1 and Figure \$12. An oscilloscope was employed to obtain the current and voltage waveforms. A Tektronix 2048 series oscilloscope was used with a Tektronix P6015A high-voltage probe having a 1000× voltage reducing rating. A 10× current reducing probe was employed to obtain the waveforms. The approximate delivered energy to the reactor was calculated using these measurements.

The light emitted from the plasma was collected by an optical system. The emission spectra of the glow region were measured at the center of the reactor. The measurements were recorded using a dualchannel UV-VIS-NIR spectrophotometer in the scope mode (Avantes Inc., USB2000 Series). The spectral range was from 200 to 1100 nm using a line grating of 600 lines/mm and a resolution of 0.4 nm. A bifurcated fiber optic cable with 400 μ m was employed.

X-ray diffraction (XRD) patterns and scanning electron microscopy (SEM) images of both ZIFs are shown in Figure 2. Figure 2a shows the XRD pattern of ZIF-8 displaying the known sodalite phase of this ZIF. Figure 2b shows ZIF-8 displaying a broad crystal size distribution in the 1–10 μ m range. Figure 2c illustrates the XRD pattern of ZIF-67, which is in agreement with sodalite topology too. These ZIF-67 crystals display sizes within the 0.1–0.3 μ m range, as shown in Figure

The experimental BET surface areas for ZIF-8 and ZIF-67 were 1880 and 1674 m²/g, respectively. The observed surface areas are within the typical ranges reported in the literature for these microporous crystals.

The chosen porous crystals illustrate an example of a representative microporous crystalline molecular sieve hybrid framework with similar crystallographic pore apertures. ZIF-8 is a metal-organic framework composed of zinc ions with nitrogen atoms coordinated with imidazole-based groups, resulting in a microporous crystalline structure with sodalite topology. 32 ZIF-67 is isostructural to ZIF-8, with the difference that zinc ions are replaced by cobalt ions.³² The crystallographic limiting pore aperture of both ZIFs is 3.4 Å.

RESULTS AND DISCUSSION

Plasma Catalytic Activity over ZIF-8 and ZIF-67. The experiments were initially carried out without a catalyst (plasma only). The reactions were repeated three times and run at ~94 °C (average temperature with fan) and atmospheric pressure. To understand the catalytic effect of the ZIFs and distinguish it from the case with only plasma, the catalysts were tested at a similar flow rate N_2/H_2 (1:3) as shown in Figure 3. ZIF-67 and ZIF-8 displayed ammonia synthesis rates of 26.65 μmol of NH₃/min gcat and 28.52 μmol of NH₃/min gcat,

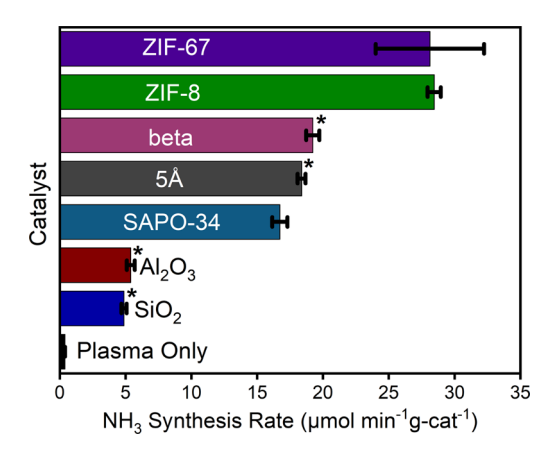


Figure 3. Ammonia synthesis rate performance for the studied ZIF crystals at 1:3 (N2:H2) feed ratio. For comparison, other zeolites $(SAPO-34, *beta, *^{27} and *5A^{27}), *oxides (Al₂O₃, SiO₂), *^{27,31} and *^{11}$ plasma only have been included.

respectively. In this figure, we compare the catalytic performance (under same reaction conditions) versus the other catalysts reported by our group such as zeolite beta,²⁷ zeolite 5A,²⁷ alumina,^{27,31} and silica.^{27,31} It is evident that both ZIFs display higher ammonia synthesis rates. When comparing with plasma only (0.386 μ mol/min), the synthesis rate is ~70 times higher with a ZIF in the reaction chamber. The active sites of the ZIFs are the -C=C- of the organic linker, which is known to be a polarizable group. The higher ammonia polarizability as compared to nitrogen and hydrogen leads to van der Waals interactions with this -C=C- group. In principle, metal sites in ZIFs may not be accessible for the guest molecules due to the steric hindrance imposed by surrounding ligands. For the studied materials, there is no direct correlation between pore size and catalytic performance. Specifically, both ZIFs have comparable limiting pore size (3.4) Å) as compared to SAPO-34 and display higher ammonia synthesis rates. SAPO-34 (SixAlyPzO₂), a chabazite zeolite displaying a pore size of ~ 3.8 Å was synthesized similar to that described in our previous report.³³ Zeolite 5A and zeolite beta having larger pore sizes (5 and ~8 Å, respectively) display comparable ammonia synthesis rates as SAPO-34. Each family of materials (ZIFs, zeolites, and oxides) has different chemistries and textural and morphological properties which affect the resultant catalytic performance.

Ammonia Adsorption on ZIF-8 and ZIF-67. To better understand the influence of adsorption properties on the catalytic behavior of the ZIF catalysts, ammonia isotherms were collected at 273 K (Figure 4). Both ZIFs display similar low ammonia uptakes. The weaker dipole-dipole interactions between the polar ammonia molecule and the polar walls of ZIFs due to the presence of uncoordinated nitrogen of the organic linker (2 methyl imidazole) lead to the lower observed ammonia uptakes. The low ammonia uptakes correlate with the high observed ammonia synthesis rates. In other words, a low concentration of ammonia is stored (uptake) with the ZIF frameworks, leading to the high ammonia synthesis rates. In the case of ZIF-8 and ZIF-67, the presence of the metal (Zn and Co, respectively) may help to promote higher ammonia synthesis rates. It is known that some transition metals are active species for ammonia synthesis via thermal catalysis. 34-36 Furthermore, Co has been identified as an effective metal for plasma catalytic ammonia synthesis. 14,15

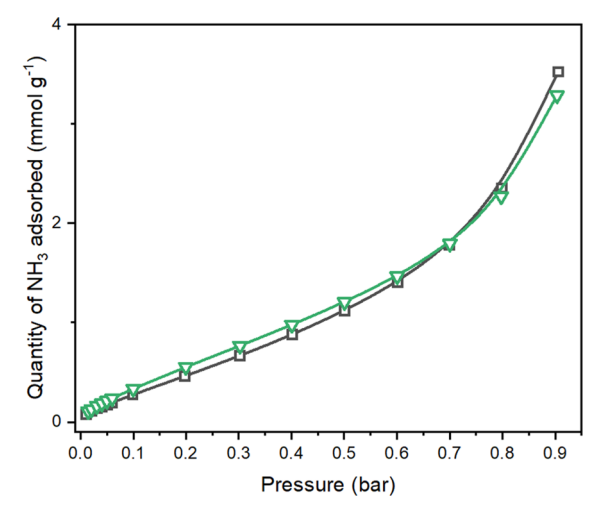


Figure 4. Ammonia isotherms collected at 273 K for ZIF-8 (square, \square) and ZIF-67 (inverted triangle, ∇).

ZIF-8 and ZIF-67 Stability. Both ZIF catalysts were recovered and recycled after the reaction. The recycling process consisted of thermal treatment at 200 °C after plasma exposure in a furnace for ~2 h. The recycled catalysts (spent) were catalytically evaluated. Figure 5 compares the perform-

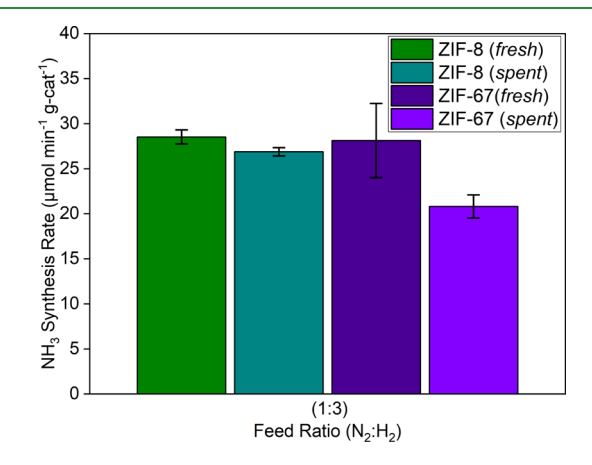


Figure 5. Ammonia synthesis rate for fresh vs. spent ZIF catalysts at 15 min and 1:3 (N_2/H_2) feed ratio.

ance of fresh versus spent catalysts at 15 min for a total flow rate of 25 sccm and 1:3 (N2:H2) ratio. ZIF-8 displayed remarkable catalytic stability after recycling. In the case of ZIF-67, a reduction of catalytic activity was observed.

XRD patterns of the spent catalysts are shown in Figure 6. For both spent ZIFs, the XRD patterns remained similar to their respective fresh catalysts. In other words, the structural stability of both ZIFs was preserved after plasma treatment. Furthermore, the morphology of the spent crystals remained the same (Figure S4), confirming the stability of both ZIFs.

ZIFs are one of the most chemically stable metal-organic frameworks. Their remarkable stability relates to the strength of their metal-ligand bond. Stable metal-organic frameworks are formed by the coordination of soft divalent cations such as Zn^{2+} and Co^{2+} with imidazolates. 37 In the case of the spent ZIF-67 sample, a minor shift of the XRD peaks to lower 2 theta angles suggests unit cell expansion. This unit cell expansion for the ZIF-67 spent sample led to higher ammonia uptakes as shown in Figure 7, resulting in lower ammonia synthesis rates.

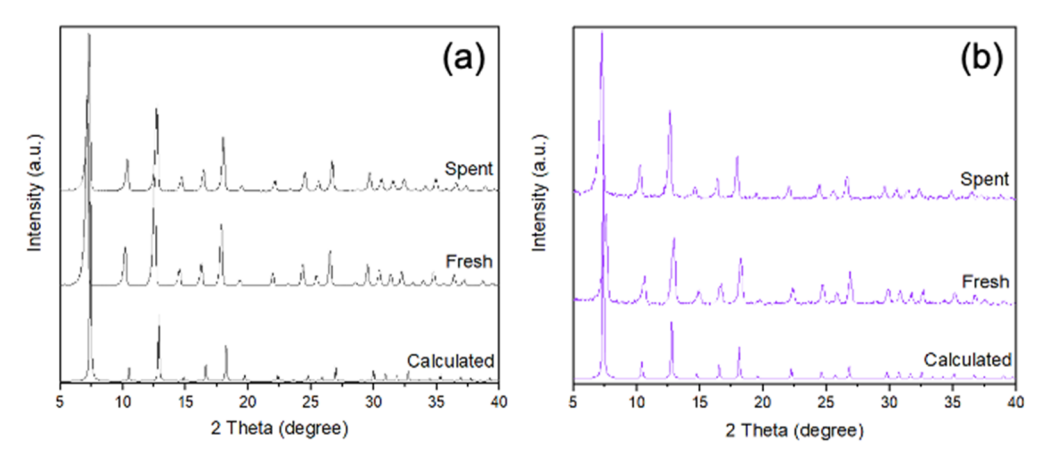


Figure 6. XRD pattern for (a) ZIF-8 and (b) ZIF-67 samples; fresh, spent, and simulated pattern tested at 1:3 (N₂/H₂) ratio.

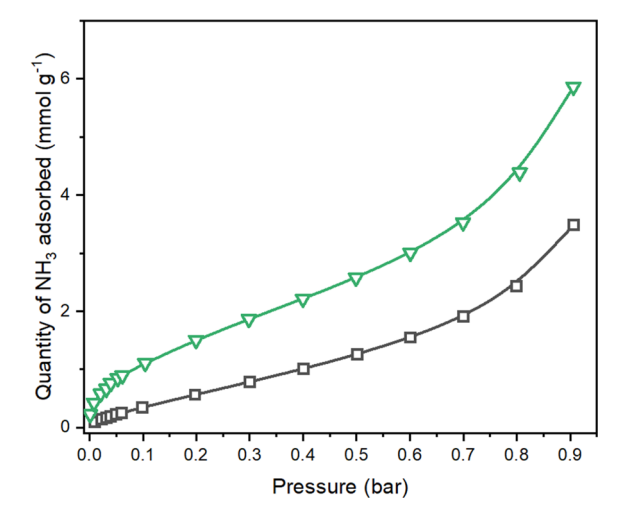


Figure 7. Ammonia isotherms collected at 273 K for spent ZIF-8 (square, \square) and spent ZIF-67 (inverted triangle, ∇).

In the case of the spent ZIF-8 sample, the ammonia uptake remained constant, which agrees well with the minimum catalytic decay of the ZIF-8 spent sample. Figure 7 shows the ammonia isotherms for fresh and spent ZIFs. Details on kinetics data for the spent materials are summarized in Figures S2–S4.

The BET nitrogen surface areas for both spent ZIFs slightly decreased. Specifically, for ZIF-8, the surface area for the fresh versus the spent sample decreased from 1880 to 1750 m²/g (~7% decrease). This slight decrease in surface area correlates with the minor catalytic decay for the spent ZIF-8 sample. In the case of the ZIF-67 sample, a more significant surface area decrease was observed for the spent sample correlating with the catalytic decay of ZIF-67 spent sample too. Specifically, the surface area of the ZIF-67 fresh sample was 1674 m²/g, and it decreased to 1305 m²/g for the spent ZIF-67 sample. Figure S5 shows the nitrogen adsorption-desorption isotherms for both ZIFs. The remarkable structural (XRD), morphological (SEM), and textural (surface area, ammonia adsorption isotherm) stability of the spent ZIF-8 sample agrees well with its stable catalytic performance before and after plasma exposure.

Optimizing the Plasma Environment. One of the main challenges when dealing with a DBD atmospheric reactor is the non-uniformity of the plasma. In fact, the optimization of the plasma environment is one of the grand challenges to

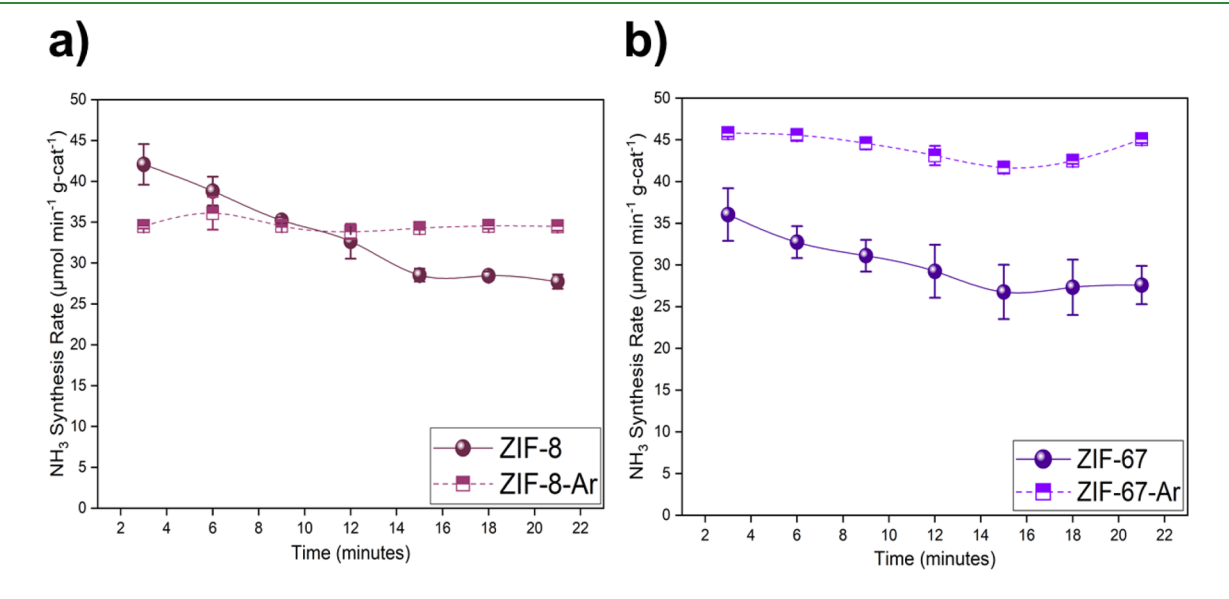


Figure 8. Ammonia synthesis rate performance for (a) ZIF-8 and (b) ZIF-67 crystals at 1:3 (N₂/H₂) feed ratio and 1:1.5:1.5 (N₂/H₂/Ar).

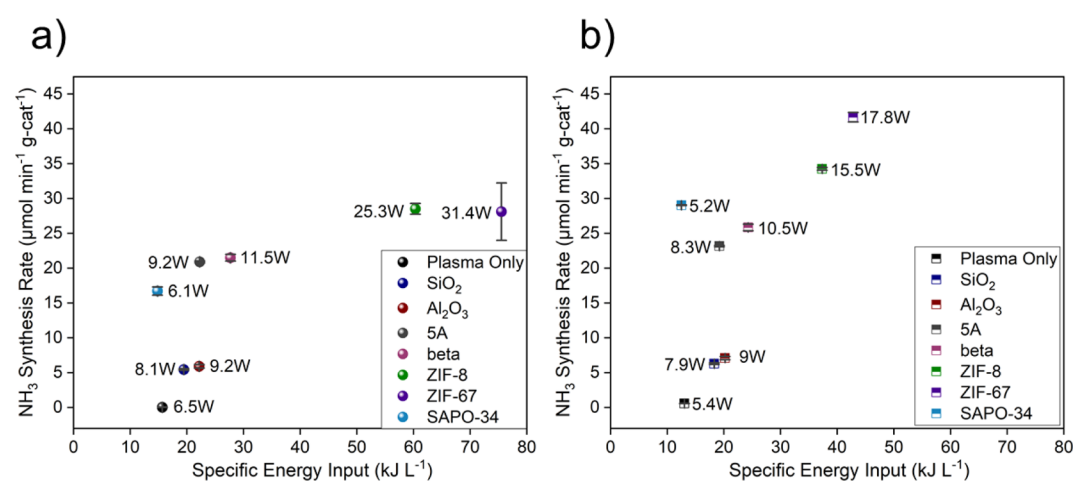


Figure 9. Specific energy input (kJ/L) vs. ammonia synthesis rate for ZIF-8, ZIF-67, SAPO-34, plasma only, $5A^*$, beta*, $Al_2O_3^*$, and $SiO_2^{*27,31}$ (a) with (1:3) (N_2/H_2) and (b) with argon dilution (1:1.5:1.5) $(N_2/H_2/Ar)$.

overcome in order to improve the plasma-mediated ammonia synthesis. The use of noble gases such as argon (Ar) is a strategy that has been employed to improve plasma homogeneity. 19,38 Therefore, we introduced Ar to the chamber at a ratio of 1N₂: 1.5H₂: 1.5Ar. The presence of Ar can increase the plasma discharge intensity and uniformity. 19 This might be attributed to the charge-transfer reaction between Ar+ and N2. The plasma homogeneity induced by the presence of Ar results in a higher probability of having electrons with the energy necessary to activate the N2 molecule. Therefore, a reduction in the required energy can be achieved since the power for reactant activation might be employed more efficiently. Interestingly, as shown in Figure 8, we observed an increase in the ammonia synthesis rate when employing Ar. For instance, at 15 min, the ammonia synthesis rates in the presence of Ar increased from 28.52 to 34.27 µmol of NH₃/ min gcat for ZIF-8 and from 28.12 to 41.68 µmol of NH₃/min gcat for ZIF-67. Furthermore, the presence of Ar stabilized the ammonia synthesis rate as a function of time. Additional data when using the feed ratio 1 N₂:1.5 H₂ was obtained to visualize the effect of argon addition in the catalytic performance (Supporting Information, Figure S6.). When looking at this data, it is evident that the ammonia synthesis rate is the highest for both ZIFs (ZIF-8 and ZIF-67) when employing N2: H2: Ar (1:1.5: 1.5) with values of 20.24 μ mol min⁻¹ g-cat⁻¹ for ZIF-8 and 24.91 μ mol min⁻¹ g-cat⁻¹ for ZIF-67. When reducing the hydrogen content for both ZIFs, that is,, $N_2:H_2$ (1:1.5), we did not find an important difference compared with the hydrogenrich data for both ZIFs, that is, N2:H2 (1:3). The ammonia synthesis rate for ZIF-8 at N_2 : H_2 (1:1.5) was 18.15 μ mol min^{-1} g-cat⁻¹ and 19.35 μ mol min^{-1} g-cat⁻¹ at N₂:H₂ (1:3). For the case of ZIF-67, the ammonia synthesis rate at N_2/H_2 (1:1.5) was 22.84 and 21.55 μ mol min⁻¹ g-cat⁻¹ at N₂/H₂ (1:3). However, this data demonstrates the overall positive effect of Ar addition.

The benefit of employing noble gases together with small particle size catalysts has been demonstrated in other plasma catalytic syntheses involving CO₂ reduction in packed beds.³⁹ This report demonstrated that the addition of Ar to CO₂ reduces the burning voltage of the mixtures, allowing discharges to form in packed void spaces at lower voltages that would typically occur in pure CO₂. ²⁴ In our case, a similar

beneficial effect in the discharge may be achieved when adding

Figure 9 compares the ammonia synthesis rate versus (specific energy input) SEI (kJ/L) for several fresh catalysts (including the studied ZIFs) evaluated at the same 1:3 (N₂/ H₂) ratio when employing the same reaction system. The SEI in kJ/L is the measured power in kW divided by the input flow ratio to the reactor in liters per minute (for power measurement details, refer to Figure S7)

SEI (kJ/L) = power (kW)/flow rate (L/min)

$$\times$$
 (60 s/1 min)

It is evident from Figure 9 that in ZIF-8 and ZIF-67, the measured watts are lower when using Ar which results in lower SEI numbers. Furthermore, higher ammonia synthesis rates were observed as well, as discussed previously. ZIF-8 and ZIF-67 show the highest ammonia synthesis rates (34.27 μ mol of NH_3 /min gcat and 41.68 μ mol of NH_3 /min gcat, respectively), while the calculated SEI was 37.34 and 42.81 kJ/L for each material, respectively, when employing a mixture with argon. The SEI values and synthesis rates for these materials without argon were 60.79 kJ/L and 28.52 µmol of NH₃/min gcat for ZIF-8 and 75.52 kJ/L and 28.12 µmol of NH₃/min gcat for ZIF-67, respectively. Both ZIFs showed higher ammonia synthesis rates as compared to other materials that do not contain a metal and those which were explored by our group previously. 26,27,31 However, it should be noted that when employing ZIF-8 and ZIF-67, the ammonia synthesis rates are not very different within the experimental error range. This suggests that the topology and textural properties (among other properties) of the ZIFs, play a more important role in the plasma catalytic synthesis of ammonia than the transition metal itself. Argon dilution resulted in an enhancing effect on the ammonia synthesis production for ZIFs and zeolites. However, there was no evident change detected in the performance of oxides when adding argon (see Figure 9).

Emission Spectroscopy Analysis. To gain a better understanding of the role of the plasma gas-phase species in the synthesis of ammonia, optical emission spectra were collected at the feed ratio 1:3 (N2:H2) for ZIF-67 with and without Ar (Figure 10). We chose ZIF-67 due to its better catalytic performance as compared to the other microporous

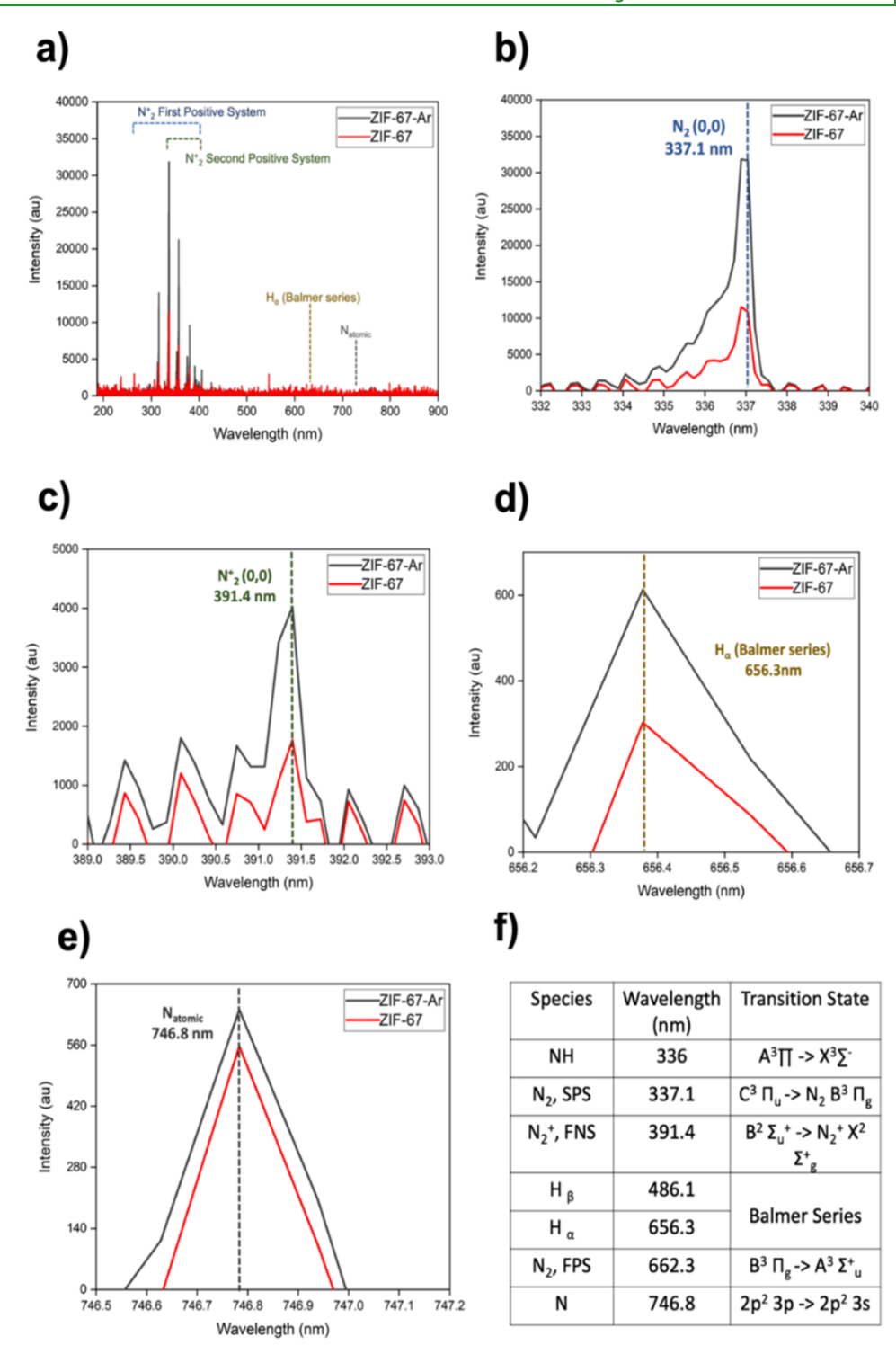


Figure 10. ZIF-67 emission spectra collected during plasma catalytic ammonia synthesis. (a) Comparative analysis of ZIF-67 at 1:3 N_2/H_2 feed ratio and diluted 1:1.5:1.5 $N_2/H_2/Ar$ feed ratio at a constant frequency of 25 kHz, (b) emission spectra of N_2 , (c) emission spectra of N_2^+ , (d) emission spectra of H_{ov} (e) emission spectra of N_{atomic} and (f) summary of important plasma species.

crystals. It can be observed that the registered peaks when using Ar are about two times more intense than without Ar. The data shown in Figure 10 was collected at equal applied voltages and the same frequency. The identification of N atomic species $(2p^23p \rightarrow 2p^23s)$ and $H\alpha$ Balmer atomic species suggest the dissociation of both N_2 and H_2 . This has been reported for ammonia synthesis in a DBD. The N_2^+ plasma-excited species (337.1 and 391.4 nm) show higher intensity values compared to atomic nitrogen (746.8 nm).

Moreover, we observed that with the addition of Ar, the formation of N_2^+ increased as observed in the UV-vis spectra. This N_2^+ plasma-excited species intensity is around 2 times higher with Ar than without Ar. The nonthermal plasma approach herein presented is focused on maximizing the density of mildly plasma-activated nitrogen species that require lower energy input as compared to nitrogen radicals. These results suggest that the presence of Ar favors a higher concentration of nitrogen vibrational species that require

lower activation energy than atomic nitrogen. Typically, mild activation of nitrogen can be achieved at relatively low SEI values, which agrees well with our results shown in Figure 9.

Constant Energy Input Experiments. We carried out selected experiments at two constant watt conditions of 5 (7– 8 kV_{pk-pk}) and 10 W (9.8–11 kV_{pk-pk}). Note that previous data presented in this paper was obtained at 25 kHz constant frequency for 15 W (12–15 kV_{pk-pk}) to 35 Ws (18–21 kV_{pk-pk}). By forcing the input energy (watts) to 5 and 10 W, respectively, we were able to observe that at constant watts, again ZIF-67 with a mixture of 1:1.5:1.5 N₂/H₂/Ar feed ratio performs the best. Hence, it is the most energy efficient (as compared to ZIF-8). Specifically, at 5 W, ZIF-67-Ar produced 20.04 μmol of NH₃/min gcat, and at 10 W, ZIF-67-Ar produced 24.91 micromoles of NH3/min gcat. Constant energy input experiments are summarized in Figure 11. We

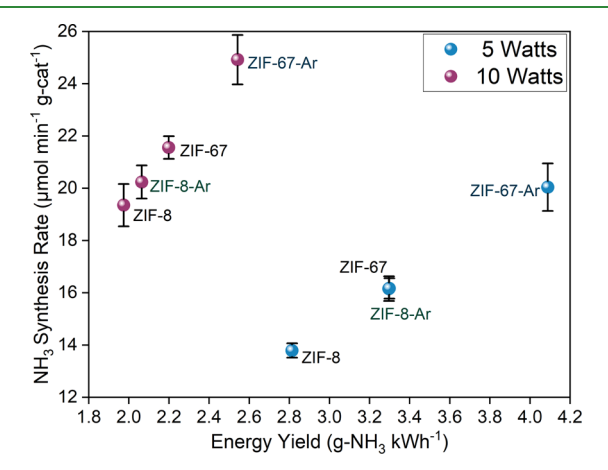


Figure 11. Ammonia synthesis rate as a function of energy yield (g-NH₃/kW h) evaluated at 1:3 (N₂/H₂) feed ratio and two constant watts conditions: 5 and 10 W.

studied the effect of nitrogen conversion (%) on the energy efficiency (%) for ZIF-67 at various discharge powers ranging from 5 to 20 W at 1:3 (N₂/H₂). With higher discharge power, the nitrogen conversion was observed to be higher, but the energy efficiency (%) was very low, as presented in Figure 12.

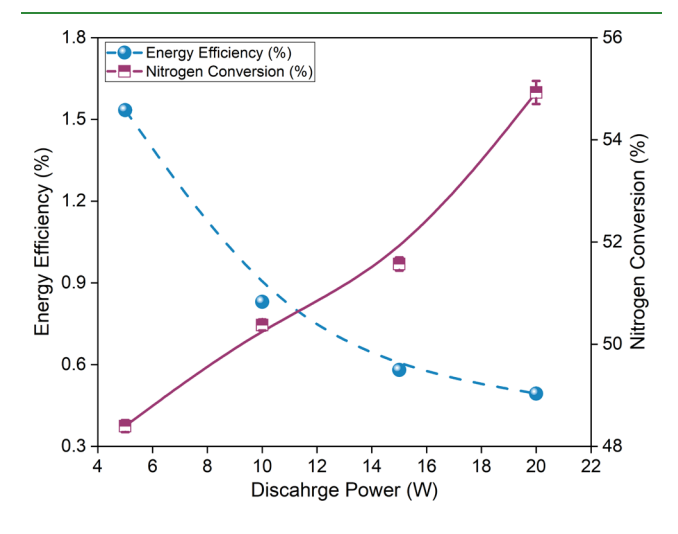


Figure 12. Nitrogen conversion (%) vs energy efficiency (%) evaluated at 1:3 (N₂/H₂) feed ratio for ZIF-67 at various constant discharge powers ranging from 5 to 20 W.

This might be indicating that the energy input is not efficiently employed towards ammonia production. Also, lower discharge powers should be preferred. The effect of micropores was studied through on-off plasma experiments to understand the ammonia desorption effect due to the presence of a high surface microporous catalyst. Figure S7 shows these experiments. It is evident that after achieving steady state and shutting down the plasma, we can observe a slight spike in the synthesis rate (at 18 and 42 min), which could possibly be attributed to the ammonia desorption from the micropores of ZIF-67. This slight increase when plasma is off can suggest the benefit of the ZIF as an NH3 storage medium avoiding the exposure of ammonia for further electron collision and decomposition. It also points out to a pulsed strategy that can benefit ammonia production and energy consumption.

Energy efficiency (%)

$$= \frac{N_2 \left(\frac{l}{\min}\right) \times N_2 \left(\%\right) \times \Delta H \left(\frac{kJ}{\min}\right)}{60 \left(\frac{s}{\min}\right) \times 22.4 \left(\frac{1}{\min}\right) \times \text{discahrge power } \left(\frac{kJ}{s}\right)}$$
(1)

To determine the main difference in the gas phase when having the extreme performing points, that is, only plasma and ZIF-67, we collected the optical emission spectra of the DBD at the feed ratio 1:3 (N_2/H_2) for only plasma and ZIF-67 with and without Ar (Figure 13). These emission spectra were collected at the constant energy input of 10 W (9.8-11 kV_{pk-pk}). Interestingly, the ZIF-67 and only plasma with Ar showed the highest intensity peaks for N_2 (337.1 nm) and N_2 (391.4 nm) in comparison with the gas phase with no Ar under the same conditions. One should recall that N_2^+ (391.4 nm) is considered one of the most important nitrogen precursors in the plasma catalytic ammonia synthesis. The intensity of N_2 (391.4 nm) was observed to be higher when Ar is in the chamber than when it is absent. The OES is a signature of the plasma gas phase, with the ammonia leading surface reactions mainly occurring on the catalyst surface. When comparing only plasma with Ar (plug flow reactor) versus ZIF-67 without Ar (packed bed reactor) (Figure 13), the N₂⁺ intensity for plasma only with Ar is higher than the intensity for ZIF-67 without Ar. Despite the intensity of N₂⁺ in the gas phase being lower for ZIF-67 without Ar, the ammonia synthesis rate is higher than only plasma with Ar (24.92 vs 0.71 μ mol min⁻¹). This can be seen as experimental proof of the plasma-catalyst synergism, showing that the presence of a catalyst plays an important role in improving the synthesis product. Also, the hydrogen content is higher with ZIF-67 without Ar N₂: H₂ (1:3) versus only plasma with Ar $N_2/H_2/Ar$ (1:1.5:1.5). The importance of hydrogen has been reported in our previous works. 35,41

CONCLUSIONS

In summary, we demonstrate that ZIF-8 and ZIF-67 microporous crystals can act as efficient catalysts for the plasma catalytic synthesis of ammonia using an atmospheric DBD reactor. Specifically, we studied two prototypical ZIFs denoted as ZIF-8 and ZIF-67 with a crystallographic pore size of 3.4 Å. The studied ZIFs displayed ammonia synthesis rates as high as 42.16 µmol NH₃/min gcat. ZIF-8 displayed remarkable stability upon recycling. The dipole-dipole interactions between the polar ammonia molecule and the polar walls of ZIF-8 and ZIF-67 led to relatively low ammonia storage capacity and therefore to high observed ammonia

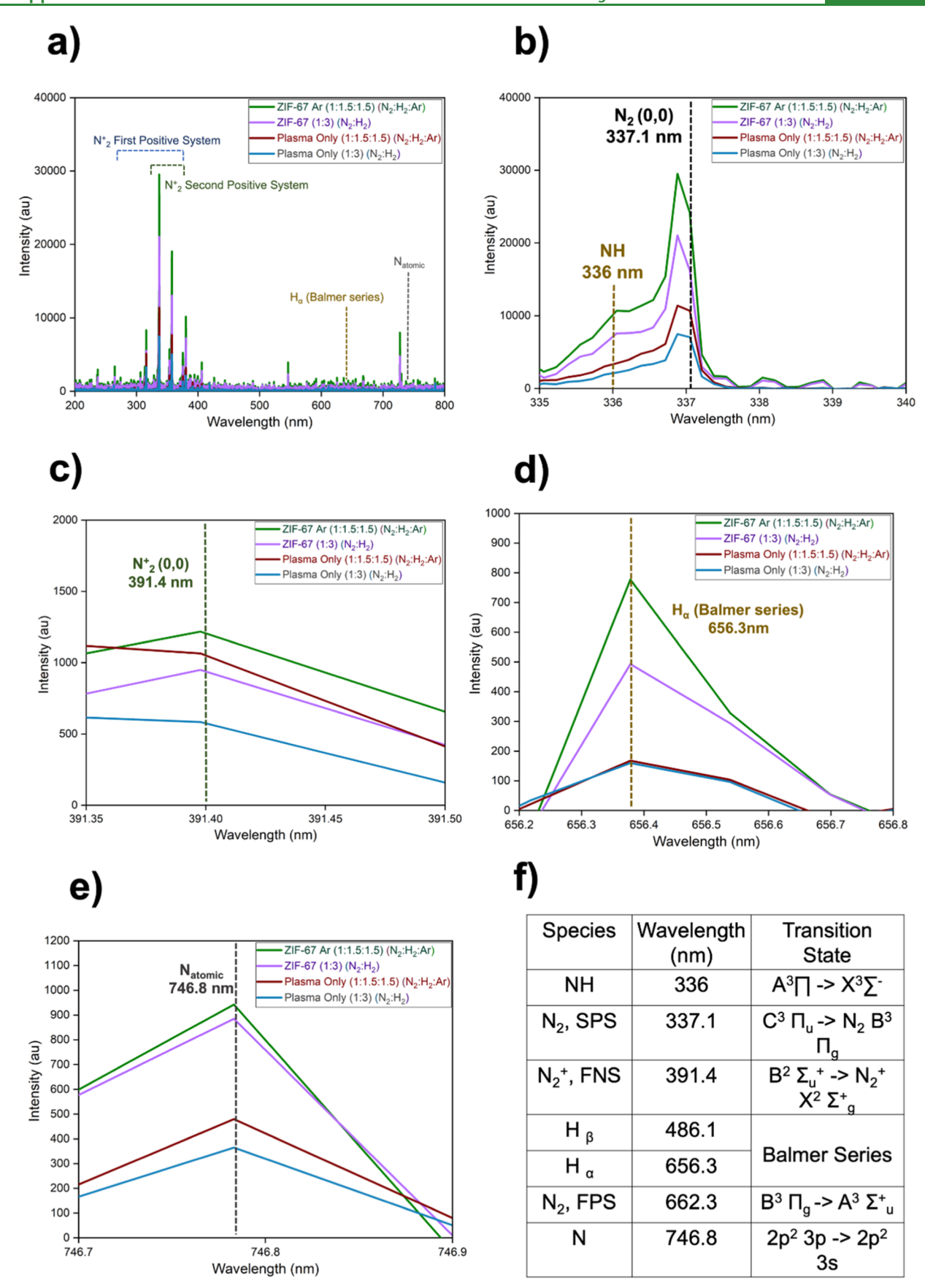


Figure 13. Emission spectra collected during plasma catalytic ammonia synthesis. (a) Comparative analysis on plasma only and ZIF-67 at 1:3 N_2/H_2 feed ratio and diluted 1:1.5:1.5 $N_2/H_2/Ar$ feed ratio at constant watts of 10 W, (b) emission spectra of N_2 , (c) emission spectra of N_2^+ , (d) emission spectra of H_{av} (e) emission spectra of N_{atomic} and (f) summary of important plasma species.

synthesis rates. The studied ZIFs outperform other microporous crystals, including zeolites and traditional oxides, in ammonia synthesis rates. To improve plasma uniformity, argon was introduced in the reaction chamber. The presence of argon resulted in synthesis rates ~1.2 times higher than without argon for both ZIFs. Moreover, the calculated SEI values were ~1.6 times smaller with argon. These lower observed SEI values translated into a higher concentration of plasma vibrational activated nitrogen species that require lower energy than atomic nitrogen. Therefore, argon improved the energy efficiency of the reaction system by allowing its operation in a low SEI range allowing the formation of less energy-consuming nitrogen vibrational species.

ASSOCIATED CONTENT

Supporting Information

The Supporting Information is available free of charge at https://pubs.acs.org/doi/10.1021/acsami.1c03115.

Details on ammonia calibration curve, performance of spent materials SEI vs synthesis rate, performance of spent materials with and without argon, SEM images for the spent catalyst, nitrogen adsorption-desorption isotherms, ZIF performance at various feed ratios, reactor electrical characterization, ammonia synthesis mechanism plot, and details on reactor electrical characterization with Lissajous curve for plasma only, ZIF-8, and ZIF-67 (PDF)

AUTHOR INFORMATION

Corresponding Author

Maria L. Carreon - Chemical and Biological Engineering Department, South Dakota School of Mines & Technology, Rapid City 57701, South Dakota, United States; orcid.org/0000-0002-2717-1577;

Email: Maria.CarreonGarciduenas@sdsmt.edu

Authors

Fnu Gorky - Chemical and Biological Engineering Department, South Dakota School of Mines & Technology, Rapid City 57701, South Dakota, United States

Jolie M. Lucero - Chemical and Biological Engineering Department, Colorado School of Mines, Golden 8040, Colorado, United States; o orcid.org/0000-0002-4606-

James M. Crawford – Chemical and Biological Engineering Department, Colorado School of Mines, Golden 8040, Colorado, United States; o orcid.org/0000-0003-3614-

Beth Blake - Chemical and Biological Engineering Department, South Dakota School of Mines & Technology, Rapid City 57701, South Dakota, United States

Moises A. Carreon - Chemical and Biological Engineering Department, Colorado School of Mines, Golden 8040, Colorado, United States; o orcid.org/0000-0001-6391-2478

Complete contact information is available at: https://pubs.acs.org/10.1021/acsami.1c03115

Notes

The authors declare no competing financial interest.

ACKNOWLEDGMENTS

M.L.C. thanks NSF-CBET award no. 1947303 and M.A.C. acknowledges the Department of Energy, Office of Science, DE-SC0021357. We thank Prof. Manika Prasad and graduate student Gama Firdaus from the Colorado School of Mines, Geophysics Department, for their support with adsorption measurements.

REFERENCES

- (1) Tanabe, Y.; Nishibayashi, Y. Developing more Sustainable Processes for Ammonia Synthesis. Coord. Chem. Rev. 2013, 257, 2551-2564.
- (2) Global Ammonia Capacity to reach 250 million tons per year by 2018. http://ictpost.com/global-ammonia-capacity-to-reach-250million-tons-per-year-by-2018/ (accessed on April 26, 2021).
- (3) Erisman, J. W.; Sutton, M. A.; Galloway, J.; Klimont, Z.; Winiwarter, W. How a Century of Ammonia Synthesis changed the World. Nat. Geosci. 2008, 1, 636.
- (4) Schlögl, R. Ammonia synthesis. In Handbook of heterogeneous catalysis; Wiley-VCH, 2008, pp 2501-2575.
- (5) Patil, B. S. Plasma (Catalyst)-assisted Nitrogen Fixation: Reactor Development for Nitric Oxide and Ammonia Production; Technische Universiteit Eindhoven, 2017, pp 1–223.
- (6) Mizushima, T.; Matsumoto, K.; Ohkita, H.; Kakuta, N. Catalytic Effects of Metal-Loaded Membrane-like Alumina Tubes on Ammonia Synthesis in Atmospheric Pressure Plasma by Dielectric Barrier Discharge. Plasma Chem. Plasma Process. 2007, 27, 1-11.
- (7) Skodra, A.; Stoukides, M. Electrocatalytic Synthesis of Ammonia from Steam and Nitrogen at Atmospheric Pressure. Solid State Ionics 2009, 180, 1332-1336.
- (8) Mukherjee, S.; Cullen, D. A.; Karakalos, S.; Liu, K.; Zhang, H.; Zhao, S.; Xu, H.; More, K. L.; Wang, G.; Wu, G. Metal-Organic Framework-Derived Nitrogen-Doped Highly Disordered Carbon for Electrochemical Ammonia Synthesis using N2 and H2O in Alkaline Electrolytes. Nano Energy 2018, 48, 217-226.
- (9) Fu, R.; Feldman, D. J.; Margolis, R. M.; Woodhouse, M. A.; Ardani, K. B. US Solar Photovoltaic System Cost Benchmark: Q1 2017; National Renewable Energy Lab.(NREL): Golden, CO (United States), 2017, pp 1-59.
- (10) Hu, L.; Khaniya, A.; Wang, J.; Chen, G.; Kaden, W. E.; Feng, X. Ambient Electrochemical Ammonia Synthesis with High Selectivity on Fe/Fe Oxide Catalyst. ACS Catal. 2018, 8, 9312-9319.
- (11) Rouwenhorst, K. H. R.; Engelmann, Y.; van 't Veer, K.; Postma, R. S.; Bogaerts, A.; Lefferts, L. Plasma-Driven Catalysis: Green Ammonia Synthesis with Intermittent Electricity. Green Chem. 2020, 22, 6258-6287.
- (12) Carreon, M. L. Plasma Catalytic Ammonia Synthesis: State of the Art and Future Directions. J. Phys. D Appl. Phys. 2019, 52, 483001.
- (13) Neyts, E. C.; Ostrikov, K.; Sunkara, M. K.; Bogaerts, A. Plasma Catalysis: Synergistic Effects at the Nanoscale. Chem. Rev. 2015, 115, 13408-13446.
- (14) Mehta, P.; Barboun, P.; Herrera, F. A.; Kim, J.; Rumbach, P.; Go, D. B.; Hicks, J. C.; Schneider, W. F. Overcoming Ammonia Synthesis Scaling Relations with Plasma-Enabled Catalysis. Nat. Catal. 2018, 1, 269-275.
- (15) Barboun, P.; Mehta, P.; Herrera, F. A.; Go, D. B.; Schneider, W. F.; Hicks, J. C. Distinguishing Plasma Contributions to Catalyst Performance in Plasma-Assisted Ammonia Synthesis. ACS Sustainable Chem. Eng. 2019, 7, 8621-8630.
- (16) van't Veer, K.; Reniers, F.; Bogaerts, A. Zero-Dimensional Modeling of Unpacked and Packed Bed Dielectric Barrier Discharges: The Role of Vibrational Kinetics in Ammonia Synthesis. Plasma Sources Sci. Technol. 2020, 29, 045020.
- (17) Herrera, F. A.; Brown, G. H.; Barboun, P.; Turan, N.; Mehta, P.; Schneider, W. F.; Hicks, J. C.; Go, D. B. The Impact of Transition Metal Catalysts on Macroscopic Dielectric Barrier Discharge (DBD) Characteristics in an Ammonia Synthesis Plasma Catalysis Reactor. J. Phys. D Appl. Phys. 2019, 52, 224002.

- (18) Hong, J.; Prawer, S.; Murphy, A. B.; Murphy. Plasma Catalysis as an Alternative Route for Ammonia Production: Status, Mechanisms, and Prospects for Progress. ACS Sustainable Chem. Eng. 2018, 6, 15–31.
- (19) Hong, J.; Prawer, S.; Murphy, A. B. Production of Ammonia by Heterogeneous Catalysis in a Packed-Bed Dielectric-Barrier Discharge: Influence of Argon Addition and Voltage. *IEEE Trans. Plasma Sci.* **2014**, *42*, 2338–2339.
- (20) Patil, B. S.; Van Kaathoven, A. S. R.; Peeters, F. J. J.; Cherkasov, N.; Lang, J.; Wang, Q.; Hessel, V. Deciphering the Synergy between Plasma and Catalyst Support for Ammonia Synthesis in a Packed Dielectric Barrier Discharge Reactor. J. Phys. D Appl. Phys. 2020, 53, 144003.
- (21) Peng, P.; Li, Y.; Cheng, Y.; Deng, S.; Chen, P.; Ruan, R. Atmospheric Pressure Ammonia Synthesis using Non-Thermal Plasma assisted Catalysis. *Plasma Chem. Plasma Process.* **2016**, 36, 1201–1210.
- (22) Akay, G.; Zhang, K. Process Intensification in Ammonia Synthesis using Novel Coassembled Supported Microporous Catalysts Promoted by Nonthermal Plasma. *Ind. Eng. Chem. Res.* **2017**, *56*, 457–468.
- (23) Duan, C.; Yu, Y.; Xiao, J.; Li, Y.; Yang, P.; Hu, F.; Xi, H. Recent Advancements in Metal—Organic Frameworks for Green Applications. *Green Energy Environ.* **2020**, 1–17.
- (24) Duan, C.; Yi, Y.; Li, J.; Libo, L.; Huang, B.; Chen, D.; Xi, H. Recent Advancements in the Synthesis of Monolithic Metal—Organic Frameworks. *Sci. China Mater.* **2021**, 1–15.
- (25) Shah, J.; Wu, T.; Lucero, J.; Carreon, M. A.; Carreon, M. L. Nonthermal Plasma Synthesis of Ammonia over Ni-MOF-74. ACS Sustainable Chem. Eng. 2018, 7, 377–383.
- (26) Shah, J. R.; Gorky, F.; Lucero, J.; Carreon, M. A.; Carreon, M. L. Ammonia Synthesis via Atmospheric Plasma Catalysis: Zeolite 5A, a Case of Study. *Ind. Eng. Chem. Res.* **2020**, *59*, 5167–5176.
- (27) Gorky, F.; Carreon, M. A.; Carreon, M. L. Experimental Strategies to Increase Ammonia Yield in Plasma Catalysis over LTA and BEA Zeolites. *IOP SciNotes* **2020**, *1*, 024801.
- (28) Carreon, M. A. Porous Crystals as Membranes. *Science* **2020**, 367, 624–625.
- (29) Feng, X.; Zong, Z.; Elsaidi, S. K.; Jasinski, J. B.; Krishna, R.; Thallapally, P. K.; Carreon, M. A.; Zhaowang, Z.; Sameh, K. E.; Jacek, B. J.; Rajamani, K.; Praveen, K. T.; Moises, A. C. Kr/Xe Separation over a Chabazite Zeolite Membrane. *J. Am. Chem. Soc.* **2016**, *138*, 9791–9794.
- (30) Feng, X.; Carreon, M. A. Kinetics of transformation on ZIF-67 crystals. *J. Cryst. Growth* **2015**, *418*, 158–162.
- (31) Gorky, F.; Best, A.; Jasinski, J.; Allen, B. J.; Alba-Rubio, A. C.; Carreon, M. L. Plasma catalytic ammonia synthesis on Ni nanoparticles: the size effect. *J. Catal.* **2020**, *393*, 369–380.
- (32) Park, K. S.; Ni, Z.; Côté, A. P.; Choi, J. Y.; Huang, R.; Uribe-Romo, F. J.; Chae, H. K.; O'Keeffe, M.; Yaghi, O. M. Exceptional Chemical and Thermal Stability of Zeolitic Imidazolate Frameworks. *Proc. Natl. Acad. Sci. U.S.A.* **2006**, *103*, 10186–10191.
- (33) Zong, Z.; Feng, X.; Huang, Y.; Song, Z.; Zhou, R.; Zhou, S. J.; Carreon, M. A.; Yu, M.; Li, S. Highly Permeable N2/CH4 Separation SAPO-34 Membranes Synthesized by Diluted Gels and Increased Crystallization Temperature. *Microporous Mesoporous Mater.* **2016**, 224 36–42.
- (34) Iwamoto, M.; Akiyama, M.; Aihara, K.; Deguchi, T. Ammonia Synthesis on Wool-like Au, Pt, Pd, Ag, or Cu Electrode Catalysts in Nonthermal Atmospheric-Pressure Plasma of N2 and H2. *ACS Catal.* **2017**, *7*, 6924–6929.
- (35) Shah, J.; Wang, W.; Bogaerts, A.; Carreon, M. L. Ammonia Synthesis by Radio Frequency Plasma Catalysis: Revealing the Underlying Mechanisms. ACS Appl. Energy Mater. 2018, 1, 4824–4839
- (36) Mehta, P.; Barboun, P. M.; Engelmann, Y.; Go, D. B.; Bogaerts, A.; Schneider, W. F.; Hicks, J. C. Plasma-catalytic ammonia synthesis beyond the equilibrium limit. *ACS Catal.* **2020**, *10*, *6726*–*6734*.

- (37) Yuan, S.; Feng, L.; Wang, K.; Pang, J.; Bosch, M.; Lollar, C.; Sun, Y.; Qin, J.; Yang, X.; Zhang, P.; Wang, Q.; Zou, L.; Zhang, Y.; Zhang, L.; Fang, Y.; Li, J.; Zhou, H.-C. Stable Metal-Organic Frameworks: Design, Synthesis, and Applications. *Adv. Mater.* **2018**, 30, 1704303.
- (38) Li, S.; Van Raak, T.; Gallucci, F. Investigating the Operation Parameters for Ammonia Synthesis in Dielectric Barrier Discharge Reactors. *J. Phys. D Appl. Phys.* **2019**, *53*, 014008.
- (39) Butterworth, T.; Elder, R.; Allen, R. Effects of particle size on CO 2 reduction and discharge characteristics in a packed bed plasma reactor. *Chem. Eng. J.* **2016**, 293, 55–67.
- (40) Wang, Y.; Craven, M.; Yu, X.; Ding, J.; Bryant, P.; Huang, J.; Tu, X. Plasma-Enhanced Catalytic Synthesis of Ammonia over a Ni/Al2O3 Catalyst at Near-Room Temperature: Insights into the Importance of the Catalyst Surface on the Reaction Mechanism. ACS Catal. 2019, 9, 10780–10793.
- (41) Shah, J.; Gorky, F.; Psarras, P.; Seong, B.; Gómez-Gualdrón, D. A.; Carreon, M. L. Enhancement of the Yield of Ammonia by Hydrogen-Sink Effect during Plasma Catalysis. *ChemCatChem* **2020**, *12*, 1200–1211.